Sensors and Actuators B 254 (2018) 206–213

Contents lists available at ScienceDirect

Sensors and Actuators B: Chemical

journal homepage: www.elsevier.com/locate/snb

Ratiometric fluorescence sensor for the sensitive detection of *Bacillus thuringiensis* transgenic sequence based on silica coated supermagnetic nanoparticles and quantum dots

Long Wu [a], Jiamin Deng [a], Xuecai Tan [b], Wenmin Yin [a], Fan Ding [a], Heyou Han [a,*]

[a] State Key Laboratory of Agricultural Microbiology, College of Food Science and Technology, College of Science, Huazhong Agricultural University, Wuhan 430070, PR China
[b] School of Chemistry and Chemical Engineering, Guangxi University for Nationalities, Nanning 530008, PR China

ARTICLE INFO

Article history:
Received 2 May 2017
Received in revised form 1 July 2017
Accepted 6 July 2017
Available online 8 July 2017

Keywords:
Ratiometric fluorescence sensor
Quantum dots
Magnetic beads
Bacillus thuringiensis transgene
Fluorescence resonance energy transfer

ABSTRACT

Improving the accuracy and sensitivity of fluorescence analysis is of great importance in clinical diagnosis, environmental and food monitoring. Herein, based on fluorescence resonance energy transfer (FRET), a facile and effective ratiometric fluorescence sensor was constructed for the detection of *Bacillus thuringiensis* (Bt) special gene fragment. In this work, green quantum dots (gQDs) decorated Fe_3O_4 magnetic beads (MBs) with streptavidin (SA) were acted as donor, and gold nanoparticles (GN) modified red quantum dots (rQDs@SiO_2) with hairpin DNA as receptor. When the target sequences exist, the hairpin DNA were unfolded and subsequently captured by MBs@SiO_2@gQD-SA via biotin–SA specific interaction. By using the magnetic separation method, the hybridized composites could be easily purified for florescence tests. By this means, rQDs@SiO_2@GN could enhance the fluorescence intensity of rQDs (I_{620}) and simultaneously quench the fluorescence response of gQDs (I_{540}) via FRET. Under optimal conditions, the ratio of fluorescence intensity at 620 nm and 540 nm (I_{620}/I_{540}) showed that Bt transgene fragment detection owning a good linearity from 5.0 pM to 10 nM with a detection limit of 0.10 pM (S/N = 3). The high selectivity of the probes was also demonstrated using the single-base and three-base mismatch method.

1. Introduction

Bacillus thuringiensis (Bt) transgene, a specific DNA sequence, can produce Bt Cry proteins that can kill insect pets. Thus, it has been widely used in genetically modified (GM) technology to replace the conventional chemical pesticides [1,2]. Up to now, the cultivation of transgenic crops with exogenous Bt gene were commercially available worldwide since Bt maize has been first commercialised [3]. However, due to the possible potential risks in food security and bio-security, the cultivation of GM crops has raised environmental, food and health concerns [4,5]. Therefore, it is extremely important to develop convenient analytical methods for the selective and sensitive detection of Bt transgene in foods and environment.

Recently, many important analytical methods such as polymerase chain reaction (PCR), electrochemistry, electrochemiluminescence (ECL) and fluorescence methods have been widely used in the detection of specific DNA sequences [6–9]. Among these analytic techniques, fluorescent detection method has aroused great interests in food analysis and bioassays due to its high sensitivity and simplicity [10,11]. Numerous fluorescent probes for DNA detection have been constructed on the basis of molecular hybridization [12], enzyme catalysis [13], hydrogen bonding recognition [14] and metal ions coordination [15] and so on. Nevertheless, most of them employ a sole responsive signal for DNA detection, which may suffer from the signal fluctuation caused by variation in detection system and some external factors [16,17]. Fortunately, ratiometric fluorescence probes have the advantages of eliminating most ambiguous interference by its self-referencing of two emission peaks [18,19]. Owing to the enhanced accuracy, ratiometric fluorescence probes have attracted increasing attention in DNA detection [20,21]. But for most probes/sensors, it is a still-challenging issue to detect specific DNA sequence or low abundance gene with accuracy and sensitivity. To address the challenges, a number of novel ratiometric fluorescence sensors have been developed [22–24]. Unfortunately, most of the ratiometric flu-

* Corresponding author.
E-mail address: hyhan@mail.hzau.edu.cn (H. Han).

http://dx.doi.org/10.1016/j.snb.2017.07.021
0925-4005/

orescence probes are confined to the organic dye molecules, which suffer from disadvantages such as poor water solubility, low photo stability and quantum yield and difficult to produce [25,26]. Additionally, the organic dyes are susceptible to photo-bleaching and some of them undergo significant background fluorescence, which can cause a decrease in the sensitivity [27–29]. Therefore, it is crucial to develop signal-amplified ratiometric fluorescence probes for improving the sensitivity and accuracy based on new fluorescence materials.

In recent decades, a few inorganic fluorescence nanomaterials, such as quantum dots [30], carbon dots [31] and metal (gold and silver) nanocluster [32,33], have received increasing interests. Owing to the superior features such as excellent photo-stability, strong fluorescence intensity, easy surface modification, good size uniformity and broad wavelength tunability [34,35], quantum dots (QDs) have been considered as the ideal fluorescent probes [36]. However, one problem is that when QDs are modified or conjugated, their stability and fluorescence will decrease, and the other one is that the coupled probes are difficult to be separated from the detection system [37,38]. It was reported that silica coating could resist the influence of the external environment (pH and high salt concentrations etc.) and retain the optical properties of the original core/shell particles [38–40]. Also, due to its facile chemical processability and good stability in aqueous media, the silica surface can be easily modified to link bioconjugators such as avidin and streptavidine [41,42]. Meanwhile, a large mount of QDs were preserved with the coating of silica shell, which further promoted the signal intensity and stability [37]. Besides, it is well known that magnetic nanoparticles (MBs) have been widely used in biomedical fields, especially for magnetic immobilization and separation [43,44]. Thus, it is meaningful to design a ratiometric fluorescent probe for the sensitive detection of DNA sequence based on silica coated MBs and QDs.

In this work, we prepared the encapsulation of both Fe_3O_4 MBs and QDs with a silica shell to form hybrid materials denoted as MBs@SiO_2@gQDs and rQDs@SiO_2. Based on the two probes, a ratiometric fluorescent sensor was designed for special Bt fragment sequence detection in aqueous solution (Scheme 1). The whole structure include two steps: (1) silica coated MBs and gQDs loaded MB@SiO_2 were prepared as donor and used for convenient separation [42,45] (Scheme 1**A**); (2) silica coated rQDs (rQDs@SiO_2) and GN loaded rQDs@SiO_2 were synthesized as receptor to quench gQDs fluorescence by FRET (Scheme 1**B**). After that, the biotin tailed hairpin DNA was attached onto rQDs@SiO_2. Then MBs@SiO_2@gQDs was conjugated with SA to capture rQD@SiO_2 for convenient separation. In the absence of target DNA (tNDA), only the fluorescence signal of gQDs appeared as the stem-loop structure was closed and the biotin was masked. If the tNDA exists, the loop of hairpin DNA would hybridize with the tNDA and opened the hairpin so as to be captured by MBs@SiO_2@gQDs, which led to the increase of rQDs fluorescence intensity (I_{620}) and the decrease of gQDs fluorescence intensity (I_{540}) (Scheme 1**C**). The ratio of the fluorescence intensity (I_{620}/I_{540}) behaved a good linearity and high sensitivity for Bt transgene detection. Hence, the ratiometric fluorescent sensor is expected to be a useful analytical tool for detection of specific DNA sequences in environmental and food monitoring.

2. Material and methods

2.1. Chemicals and materials

Water and oil CdSe/ZnS QDs (gQDs: 540 nm; rQDs: 620 nm) were purchased from Xingzi (Shanghai) New Material Technology Development Co., Ltd; SA and the oligonucleotides (Table S1) used in the work were purchased from Shanghai sangon Biotechnology Co., Ltd. All chemicals and solvents were of analytical grade and used without further purification. Ultrapure water obtained from Milli-Q, Millipore (18.2 MΩ resistivity) was used throughout the experiment.

2.2. Instrumentation

Photoluminescence (PL) spectra were acquired on Edinburgh FLS920 spectrometer under an excitation of 360 nm; Zeta potential and hydrodynamic size were measured by dynamic light scatting (DLS) using a Malvern Zeta Sizer (Nano-ZS) system. Transmission electron microscope (TEM) images were taken on a JEM-2010FEF transmission electron microscopy at an accelerating voltage of 200 kV.

2.3. Synthesis and modification of MBs@SiO_2@gQDs-SA

To obtain MBs@SiO_2@gQDs composites, MBs@SiO_2 (MS) was first synthesized according to previous work [45,46]. Next, SA and CdSe/ZnS QDs (gQDs: 540 nm) were introduced to obtain MS@gQDs-SA composites. The detailed procedures were provided in Supplementary information.

2.4. Synthesis and functionalization of rQDs@SiO_2@GN-H3

rQDs@SiO_2 and gold nanoparticles (GN) loaded rQDs@SiO_2 were first prepared based on previous work with some changes [47–49]. Then the capture DNA (H3) was attached on the rQDs@SiO_2@GN via Au-S bond to form the rQDs@SiO_2@GN-H3 composites. The final product was stored in PBS buffer solution (pH = 7.4) at 4 °C for further use. The detailed preparation procedures were described in Supplementary information.

2.5. Construction of ratiometric fluorescent sensor

After the two different fluorescence probes were well prepared, the solution of the two probes were mixed together in a PBS buffer medium (pH = 7.4) containing 0.1 mM NaCl and 3.0 mM $MgCl_2$. To realize the aqueous solution detection, tDNA was introduced to the solution. Then the obtained mixture solution were incubated at 40 °C in a dark room for 90 min. Afterwards, the loop of H3 would hybridize with tDNA and opened the hairpin to expose the biotin, which subsequently hybridized with MS@gQDs-SA via biotin–SA specific interaction. The recognition of the two probes led to the increment of rQDs fluorescence intensity (I_{620}) and the decrease of gQDs fluorescence intensity (I_{540}) (Scheme 1**C**). Finally, the excess rQDs@SiO_2@GN-H3 was separated and removed by an external magnetic field and the remaining solution was collected for fluorescent measurements.

3. Results and discussion

3.1. Characterization of materials

UV–vis absorption and FT-IR spectroscopic experiments were first carried out to investigate the MBs-based materials. As depicted in Fig. S1**A**, UV–vis analysis of MBs (curve a) and amino-functionalized MBs@SiO_2 (MS-NH_2) (curve b) revealed that MBs possess a wide and strong absorption peak at 400 nm, which was consistent with previous work [50]. However, after the conjugation of gQDs on the surface of MS-NH_2, the peak at 400 nm was vanished and a new peak of gQDs at 230 nm appeared (curve c and d), suggesting that gQDs were successfully attached on MBs@SiO_2. Meanwhile, FT-IR spectra of all Fe_3O_4-based materials (Fig. S1**B**) showed a characteristic band at 490 cm^{-1}, which was caused by the Fe—O stretching vibration (curve a, b, d). Besides, MS@gQDs

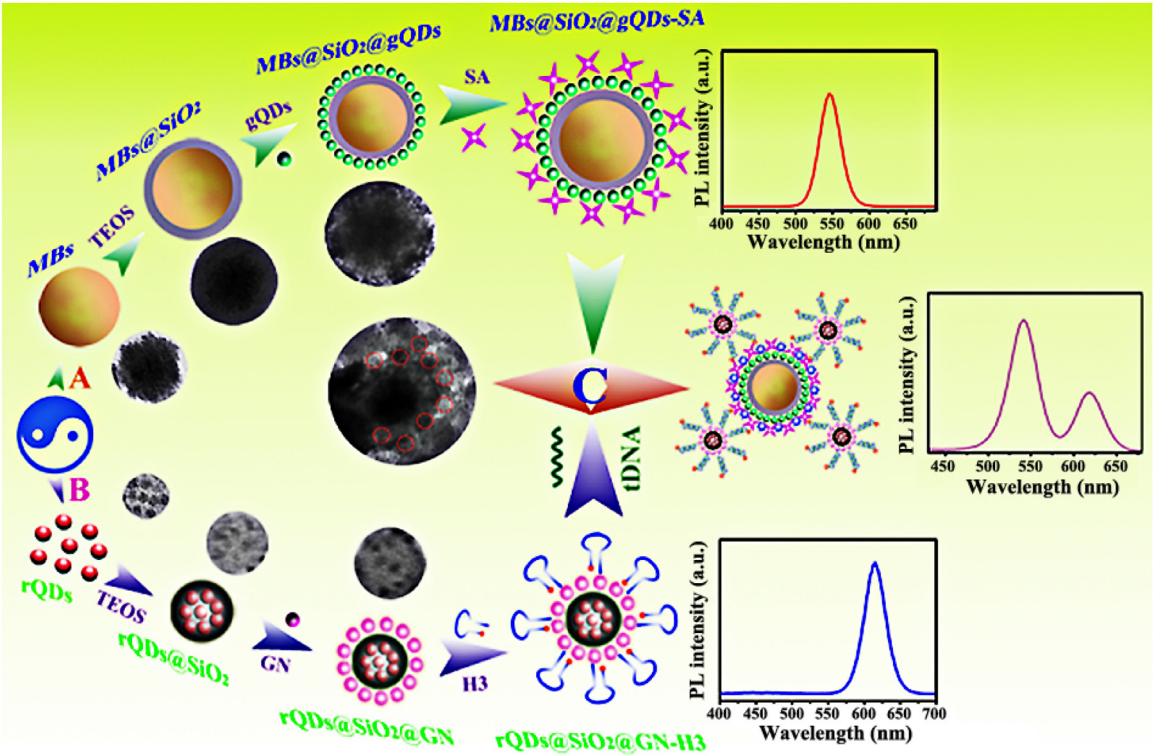

Scheme 1. Schematic illustration of the structure of ratiometric fluorescence sensor. The preparation process of (**A**) MBs@SiO_2@gQD-SA and (**B**) rQD@SiO_2@GN-H3, and (**C**) the detection of target DNA.

exhibited the FT-IR peak at 2990, 1640, 1100, and 800 cm^{-1} (curve c), revealing the successful modification of silica coating, MS-NH_2 and gQDs.

Fig. S2 described the hydrodynamic diameters of rQDs and MBs in different modification steps. As it can be seen from Fig. S2**A**, the average size of rQDs is about 3.32 nm with narrow monodispersity. After silica coating, the average size of rQDs increased to 16.63 nm (Fig. S2**B**). Next, when the rQDs@SiO_2 was further conjugated with GN, the size rapidly grew to 30.25 nm (Fig. S2**C**). The size variations reflected that rQDs were successfully coated with silica (from 3.32 to 16.63 nm) and GN were attached to the surface of rQDs@SiO_2 (from 16.63 to 30.25 nm). Similarly, as depicted in Fig. S2**D**, MBs showed good dispersity with an average size of 82.76 nm. Afterwards, the size increased to 104.52 nm after the silica coating of MBs (Fig. S2**E**) and then to 109.08 nm after amino-functionalization (Fig. S2**F**), which revealed that the silica shell thickness was about 14 nm (from 82.76 nm to 109.08 nm). Following that, after the modification of gQDs and SA, the average diameters are 181.43 nm and 208.77 nm (Fig. S2**G** and **H**), which indicated that the conjugates were successfully obtained. Finally, when MS@gQDs-SA hybridized with rQDs@SiO_2@GN-H3, the composites showed an average diameter of 280.73 nm (Fig. S2**I**), which revealed the successful construction of the fluorescence sensor. The above facts confirmed that each modification step was accomplished and the two fluorescence probes were successfully recognized in the presence of tDNA.

To discuss the surface charge of the above materials, zeta potential measurements were performed and the results were shown in Fig. S3**A**. After amino modification and conjugation with GN, it is noteworthy that the zeta potential of rQDs@SiO_2 changed from −13.6 mV to 14.0 mV and then to −15.3 mV, which revealed the successful modification of amino and GN. Besides, MS-NH_2 showed zeta potential variation from 13.8 mV to −10.6 mV after combining with gQDs, which suggested the successful surface amino functionalization and conjugation with gQDs. After the modification of SA, the zeta potential further decreased to −12.8 mV. Moreover, gel electrophoresis was adopted to investigate the molecular weights (Fig. S**3B**). The results showed that only the lane with H3 can run continuously while other samples nearly stayed at the starting line, indicating that the modified molecular are anchored strongly on the materials.

To reveal the modification step of MBs and rQDs, typical TEM images of MBs, MS, rQDs@SiO_2, rQDs@SiO_2@GN, MS@gQDs and MS@gQD/rQD@SiO_2 are all taken (Fig. 1). Fig. 1**A** indicated that MBs are well-distributed and uniform with an average size of approximately 80 nm, which is consistent with the result of DLS (Fig. S2**D**). After silica coating, the surface of MBs became smooth and the size got bigger and more uniform (Fig. 1**B**). The features of MBs and MS could also be distinguished clearly from the SEM images (Fig. S4). For the silica coated rQDs, the TEM images showed that the rQDs are incorporated with silica and form numerous individual rQDs@SiO2 particles (Fig. 1**C**). After further amino modification and attachment of GN, their size got bigger and GN are evenly dotted on rQDs@SiO_2, indicating the homogeneous distribution of GN on the silica surface (Fig. 1**D**). From Fig. 1**E**, it can be observed that numerous gQDs are loaded on the surface of MS, which indicated that gQDs were attached onto the silica surface. Moreover, the combination of MS@gQDs-SA and rQDs@SiO_2 could be recognized in Fig. 1**F**, which revealed the same results as diameter measurements (Fig. S2**H**). The TEM results indicated that the materials in Scheme 1 were successfully prepared as desired.

3.2. Verification of the magnetic and fluorescence performance

To demonstrate the advantage of magnetic separation, the magnetic response of MBs in each modification step was explored. As depicted in Fig. S5, the silica coated MBs (MS) and amino-functionalized MS (MS-NH_2) showed a high magnetic response

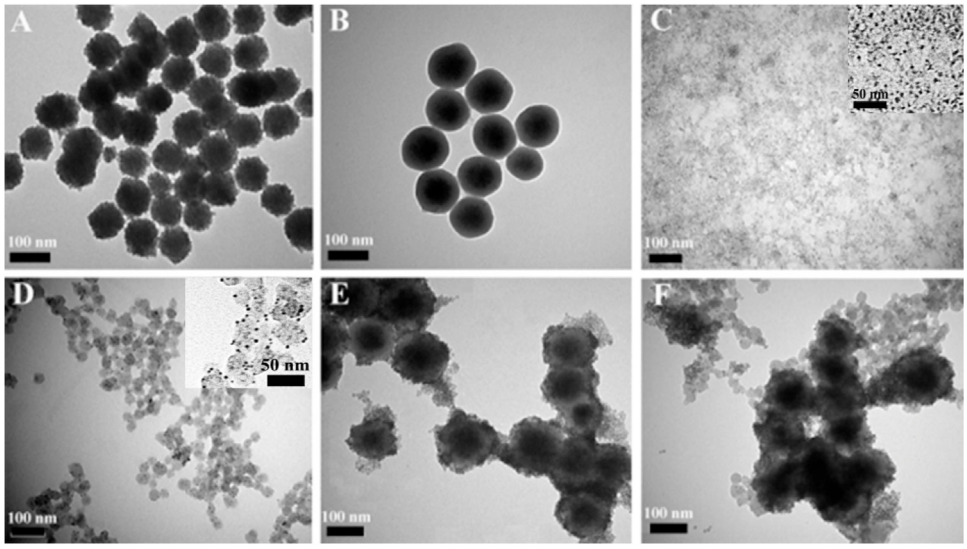

Fig. 1. TEM images of (**A**) MBs, (**B**) MBs@SiO_2 (MS), (**C**) rQD@SiO_2, (**D**) rQD@SiO_2@GN, (**E**) MBs@SiO_2@gQD (MS-gQD), and (**F**) MS@gQD/rQD@SiO_2.

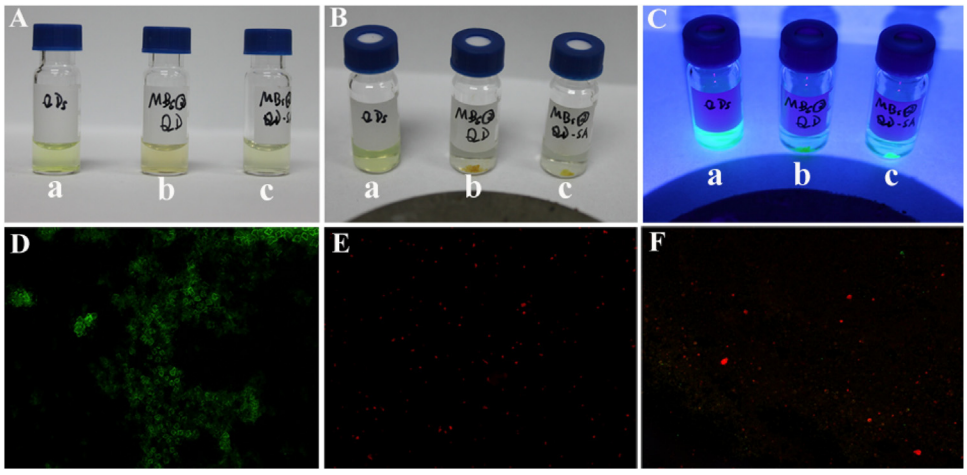

Fig. 2. Photograph of (a) QDs, (b) MS@gQDs, (c) MS@gQDs-SA in a vessel without **(A)** and with (**B**) an external magnetic field and (**C**) under ultraviolet light with magnetic field. Fluorescence microscope images of (**D**) MS@gQDs, (**E**) rQDs@SiO_2 and (**F**) MS@gQD/rQD@SiO_2 under ultraviolet excitation.

under an external magnetic field, which can be easily applied in the separation and enrichment. The performance of MS@gQDs and MS@gQDs-SA were also discussed as shown in Fig. 2. In the absence of an external magnetic field, the solution of gQDs, MS@gQDs and MS@gQDs-SA are clear and stable (Fig. 2**A**). Under the external magnetic field, gQDs still kept the same but MS@gQDs and MS@gQDs-SA were easily attracted and enriched by magnet (Fig. 2**B**). Moreover, under ultraviolet light, it can be clearly seen that the enriched MBs showed bright green fluorescence and the remaining solution are colorless (Fig. 2**C**). The results revealed that the MBs materials behaved good performance under an external magnetic field.

Fluorescence microscope images were taken to verify the fluorescence property of MS@gQDs and rQDs@SiO_2. From Fig. 2**D**, it can be seen clearly that MS@gQDs are fully covered with green fluorescence which was originated from the attached gQDs. For the silica coated rQDs (rQDs@SiO_2), it showed a mass of individual red particles under fluorescence microscope (Fig. 2**E**). The uniform particles revealed the successful silica coating of rQD. Moreover, we also investigated the fluorescence image of MS@gQDs recognized with rQDs@SiO_2. As shown in Fig. 2**F**, a composite fluorescence of green and red appeared, which indicated that rQDs@SiO_2 are attached on MS@gQDs. The fluorescence results verified that the two probes behaved good magnetic and fluorescence performance.

3.3. Fluorescence properties of the sensor

PL spectra were adopted to characterize fluorescence properties of the fluorescence probes. As depicted in Fig. 3**A**, the PL emission peak of gQDs was at 540 nm with a green emitting light (curve a). After the conjugation of gQDs on the MBs@SiO_2, the emission peak behaved a red-shift and the PL intensity slightly decreased (curve b). The red-shift could be attributed to the formation of MS@gQDs and the PL intensity decrease may be ascribed to the inadequacy conjugation of gQDs. Next, for the SA modification (curve c), it showed an inconspicuous effect on the fluorescence intensity, but a red-shift in emission was observed, which revealed the successful conjugation of SA on MS@gQDs. Fig. 3**B** showed the PL emission peak of the oil rQDs at 620 nm with an orange-red emitting light (curve a). After silica coating and amino modification, the fluorescence of rQDs decreased to a large extent but still remained high fluorescence intensity (curve b), which was consistent with previous report [47]. The attachment of GN on rQDs@SiO_2 further

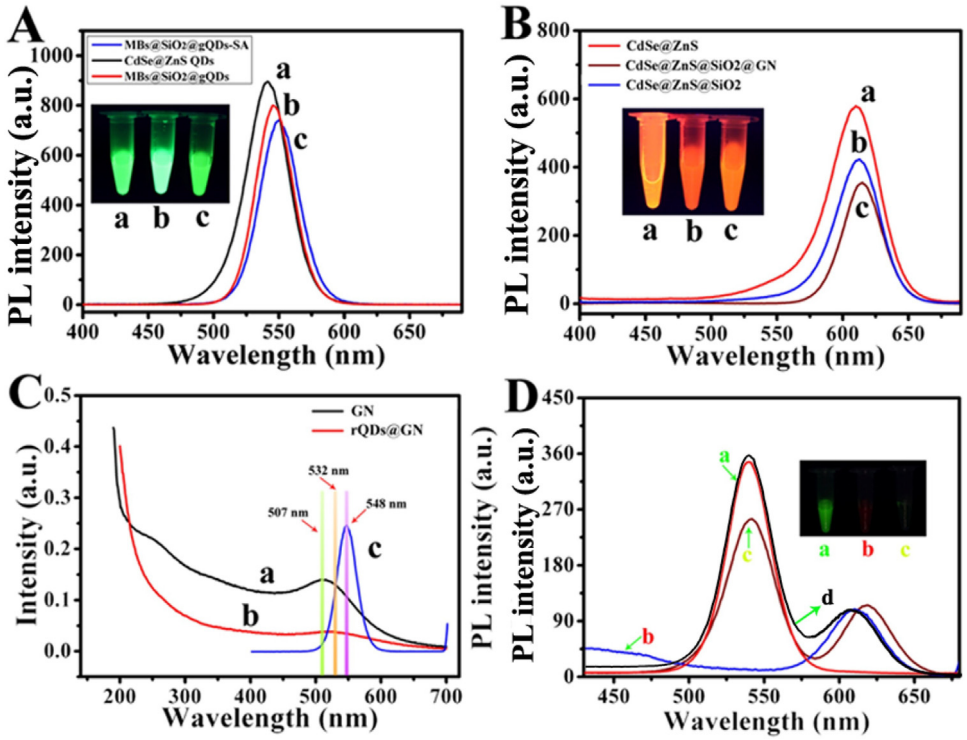

Fig. 3. Fluorescence spectra of (**A**) gQDs (a), MS@gQDs (b), MS@gQDs-SA (c) and (**B**) rQDs (a), rQDs@SiO_2 (b), rQDs@SiO_2@GN (c). (**C**) UV–vis absorption spectra and fluorescence of (a) GN and (b) rQDs@SiO_2@GN and (c) MS@gQDs-SA. (**D**) Fluorescence spectra of (a) MS@gQDs-SA, (b) rQDs@SiO_2@GN, (c) MS@gQD/rQD@SiO_2 and (d) rQDs@SiO_2@GN-H3+MS@gQD-SA.

reduced the fluorescence intensity and triggered a red-shift (curve c).

UV–vis absorption and fluorescence spectra were collected to reveal the energy transfer between rQDs@SiO_2 and MS@gQDs. As shown in Fig. 3**C**, the UV–vis absorption spectrum of GN behaved a wide and strong absorption peak at 507 nm (curve a), which was in accordance with our previous report [42]. As the GN were attached on rQDs@SiO_2, the absorption peak showed a large red-shift to 532 nm (curve b). The broad absorption band of rQDs@SiO_2@GN makes it possible to be a good energy receptor for the donors. Meanwhile, the PL spectrum of MS@gQDs-SA exhibited an emission peak at 548 nm (curve c), which was partly overlapped with the absorption band of rQDs@SiO_2@GN. Thus, this fact revealed that rQDs@SiO_2@GN could act as the receptor to quench MS@gQDs-SA fluorescence. Furthermore, the fluorescence spectra of the two probes were also explored. As exhibited in Fig. 3**D**, the PL intensity of MS@gQDs probe was largely quenched when conjugated with rQDs@SiO_2@GN (curve a and c), and the PL intensity of the two probes nearly remained the same when they were just mixed together (curve b, c, d), which further demonstrated the FRET principle as illustrated in Scheme 1.

3.4. Optimization of the detection conditions

According to previous findings [45,51], different effect factors, such as the dosage of magnetic beads, Mg^{2+} ion strength, incubation temperature and time, were explored to get the optimal experimental conditions. Since the above conditions can greatly affect fluorescence intensity, the relative variation between I_{620} and I_{540} was used to discuss the optimal conditions.

In this work, MS@gQDs-SA both act as catcher and donor, which first capture rQDs@SiO_2@GN and then donate the energy to them. Thus, the dosage of magnetic beads could seriously influence the fluorescence intensity. As depicted in Fig. 4**A**, the volumes of MS@gQDs-SA from 100 to 500 μL were explored. The highest intensity of I_{620} occurred at 300 μL and tended to be balanced as the volume further increased. Hence, 300 μL was chosen as the optimal volume for the following experiments. For the hybridization process of H3 and tDNA, we chose 37 °C and 20 min as the optimal temperature and time according to previous report [45]. Besides, it was reported that Mg^{2+} could affect the hybridization between intermolecular and intramolecular [51]. Fig. 4**B** exhibited the lowest intensity of I_{540} and the highest of I_{620} as Mg^{2+} concentration is 5 mM. However, when Mg^{2+} concentration is 3 mM, the intensity of I_{620} reached plateau but that of I_{540} still decreased. Therefore, to balance the hybridization intensity, 4 mM was adopted as the optimal concentration in the following study.

Also, the incubation temperature and time for MS@gQDs-SA and rQDs were explored. As shown in Fig. 4**C**, the lowest intensity of I_{540} and the highest of I_{620} was obtained at 35 °C. Thus, 35 °C was chosen as the optimal incubation temperature. Next, the incubation time was discussed as shown in Fig. 4**D**. The intensity of I_{620} increased and that of I_{540} decreased as the incubation time prolonged from 10 to 120 min. Obviously, both of I_{620} and I_{540} showed insignificant changes at 90 min, which indicated that the reaction between biotin and SA reached a balance state. Therefore, 90 min was selected as the optimal incubation time.

3.5. Selectivity and stability of the sensor for Bt sequence

To demonstrate the selectivity of the sensor, as here proposed, target detection in a homogeneous solution was used and the base mismatched DNA were carried out as control. In the conventional specificity analysis, three different DNA sequences were usually discussed, including complementary tDNA, single-base mismatched DNA and three-base mismatched DNA [52]. As shown in Fig. 5**A**, compared with the base mismatched DNA and the random DNA sequence, complementary sequence showed much

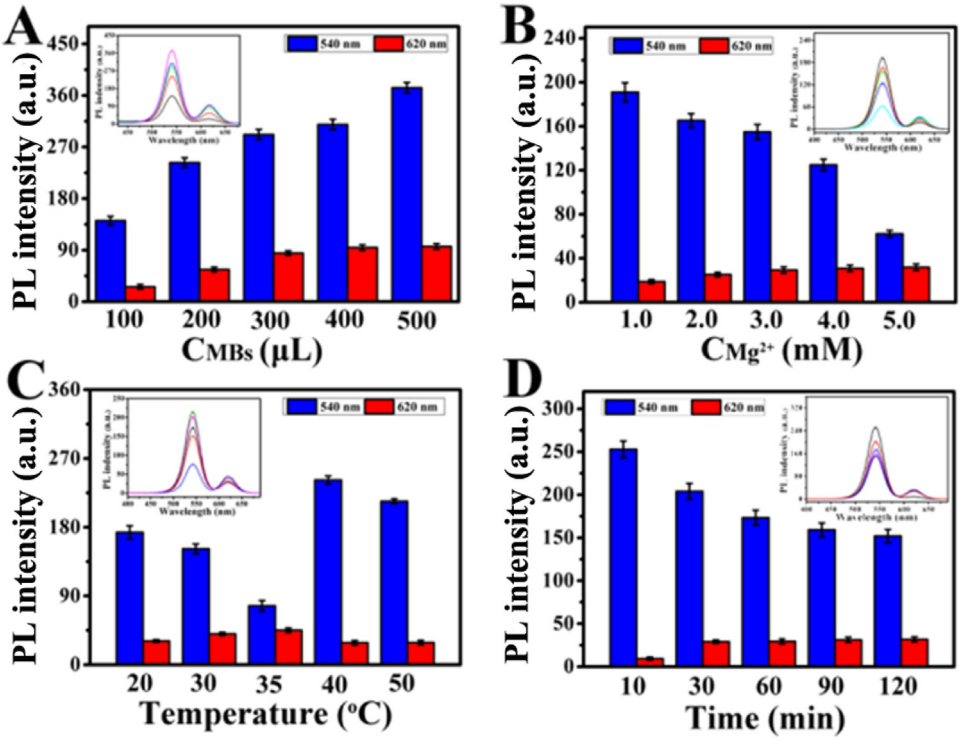

Fig. 4. The effect of different conditions on fluorescence intensity: (**A**) dosage of MS@gQDs-SA, (**B**) concentration of Mg^{2+}, (**C**) incubation temperature and (**D**) capture time. All the error bars were calculated based on the standard deviation of three measurements.

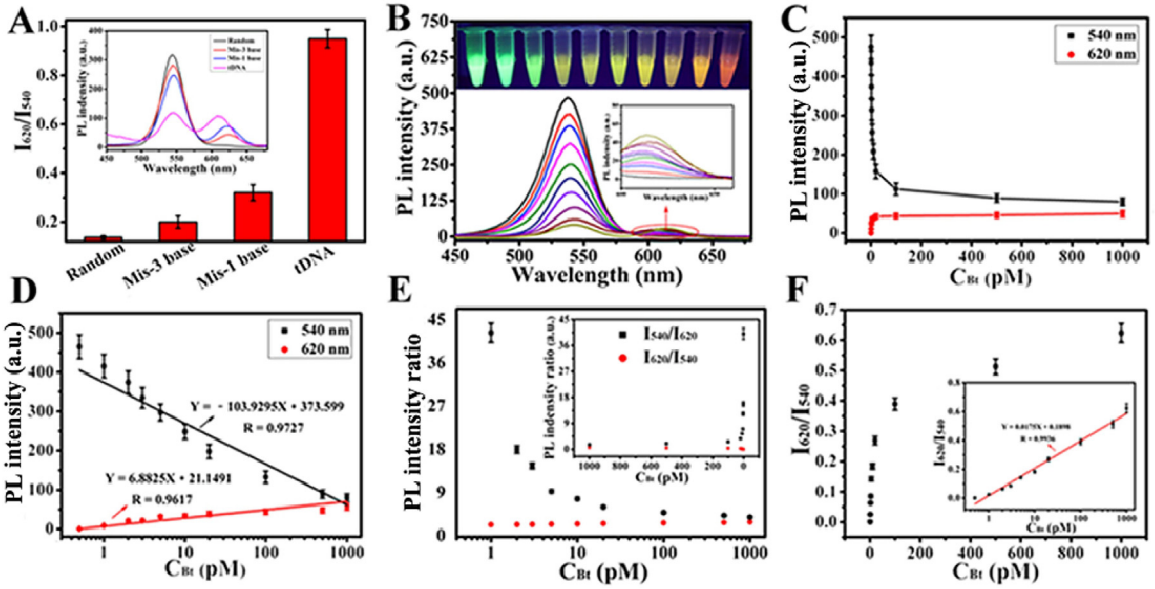

Fig. 5. (**A**) Comparison of I_{620}/I_{540} value of the sensors hybridized with tDNA, one-base mismatched tDNA, three-base mismatched tDNA and random sequence DNA in the same concentration (0.1 nM). (**B**) The detection results of different tDNA concentration based on ratiometric fluorescence sensor. (**C**) The fluorescence intensity plots of different concentrations of tDNA (from 5.0 pM to 10 nM) corresponding to the results of (**B**). (**D**) Calibration curve of I_{620}/I_{540}, (**E**) dual-signaling fluorescence intensity ratio of I_{620}/I_{540} and I_{540}/I_{620}, (**F**) dual-signaling fluorescence intensities of I_{620}/I_{540} (inset: calibration curve of I_{620}/I_{540} for determining different concentrations of tDNA ranging from 5.0 pM to 10 nM). All the error bars were calculated based on the standard deviation of three measurements.

higher I_{620}/I_{540} value due to the specific binding of H3 and tDNA. The results revealed that the interfering mutation sequences had insignificant influence on special Bt fragment detection, which further indicated that the proposed sensor has good hybridization efficiency and selectivity towards tDNA. Furthermore, the sensor was found to remain 90% of the original fluorescence after 7 days storage at 4 °C, suggesting the good stability of the fluorescence sensor. Therefore, it is specific and stable to use the sensor in the detection of Bt sequence fragment.

3.6. The analysis of Bt sequence

As shown in Fig. 5**B**, with the increase of tDNA, the fluorescence intensity of I_{620} increased and that of I_{540} decreased at the same time. Besides, the solution showed a color variation from green

to orange red as the concentration of tDNA sequence ranged from 0.1 pM to 1 nM. It can be seen that the more target sequence existed, the more fluorescence intensity of I_{540} decreased, and both of the fluorescence intensity tended to converged to one point (Fig. 5**C**), which meant that the I_{620}/I_{540} value tended to be balanced. Fig. 5**D** showed that the fluorescence detection results were dependent on the logarithm of Bt concentration with the respective calibration curves of I_{620} and I_{540}. The sensitivity of I_{620} and I_{540} were estimated to be 1.2 and 4.6 pM (S/N = 3), respectively. To prove the superior precision of the proposed sensor, plots of dual-signal fluorescence intensity ratio were described in Fig. 5**E**. Furthermore, it was found that the value of I_{620}/I_{540} was also linearly corresponding to the logarithm of target Bt concentration from 5.0 pM to 10 nM (Fig. 5**F**). The regression equation was put as $Y = 0.0175X + 0.1898$ with $R = 0.9936$, and the detection limit was estimated to be 0.10 pM (S/N = 3), where Y was the ratio of I_{620}/I_{540} and X was the logarithm of target Bt concentration. The lower error and signal fluctuation, higher sensitivity and R value of the dual-signal mode verify the superiority of the proposed ratiometric fluorescence detection method.

4. Conclusions

In summary, a ratiometric fluorescence sensor was successfully constructed via biotin–SA specific interaction for the detection of special Bt fragment based on FRET. In the method, MS@gQDs-SA both act as catcher and donor and rQDs@SiO_2@GN-H3 as receptor. Owing to the magnetic separation and high accuracy and sensitivity of the ratiometric fluorescence, the proposed sensor could behave simple, rapid, accurate and sensitive detection of tDNA sequence. The excess rQDs@SiO_2@GN-H3 could easily be separated from solution for recycling use via magnetic separation. All the materials can be readily prepared and modified with high stability and water-solubility. Thus, this method could provide an alternative approach for constructing FRET-based detection systems in the sensitive and selective detection of special gene sequence, revealing its potential in the risk assessment of food safety such as genetically modified food.

Acknowledgements

We gratefully acknowledge the financial support from National Key R & D Program (2016YFD0500700), National Natural Science Foundation of China (21375043, 21175051) and Scitech Innovation Foundation of Huazhong Agriculture University (2662017PY042).

Appendix A. Supplementary data

Supplementary data associated with this article can be found, in the online version, at http://dx.doi.org/10.1016/j.snb.2017.07.021.

References

[1] H. Höfte, H.R. Whiteley, Insecticidal crystal proteins of Bacillus thuringiensis, Microbiol. Mol. Biol. Rev. 53 (1989) 242–255.
[2] G. Hua, Y. Park, M.J. Adang, Cadherin AdCad1 in Alphitobius diaperinus larvae is a receptor of Cry3Bb toxin from Bacillus thuringiensis, Insect Biochem. Mol. Biol. 45 (2014) 11–17.
[3] Y. Carrière, J.A. Fabrick, B.E. Tabashnik, Can pyramids and seed mixtures delay resistance to Bt crops, Trends Biotechnol. 34 (2016) 291–302.
[4] D. Quist, I.H. Chapela, Transgenic DNA introgressed into traditional maize landraces in Oaxaca, Mexico, Nature 414 (2001) 541–543.
[5] H. Zeng, F. Tan, Y. Zhang, Y. Feng, Y. Shu, J. Wang, Effects of cultivation and return of Bacillus thuringiensis (Bt) maize on the diversity of the arbuscular mycorrhizal community in soils and roots of subsequently cultivated conventional maize, Soil Biol. Biochem. 75 (2014) 254–263.
[6] J. Mano, Y. Nishitsuji, Y. Kikuchi, S.I. Fukudome, T. Hayashida, H. Kawakami, Y. Kurimoto, A. Noguchi, K. Kondo, R. Teshima, R. Takabatake, K. Kitta, Quantification of DNA fragmentation in processed foods using real-time PCR, Food Chem. 226 (2017) 149–155.
[7] J. Wen, W. Li, J. Li, B. Tao, Y. Xu, H. Li, A. Lu, S. Sun, Study on rolling circle amplification of Ebola virus and fluorescence detection based on graphene oxide, Sens. Actuators B Chem 227 (2016) 655–659.
[8] A. Zhang, C. Miao, H. Shi, H. Xiang, C. Huang, N. Jia, A novel solid-state electrochemiluminescence sensor for atropine determination based on $Ru(bpy)_3^{2+}$/carbon nanospheres/Nafion composite film, Sens. Actuators B Chem. 222 (2016) 433–439.
[9] H. Tan, G. Tang, Z. Wang, Q. Li, J. Gao, S. Wu, Magnetic porous carbon nanocomposites derived from metal-organic frameworks as a sensing platform for DNA fluorescent detection, Anal. Chim. Acta 940 (2016) 136–142.
[10] Y. Zhou, J. Ding, T.X.Z. Liang, E.S. Abdel-Halim, L.P. Jiang, J.J. Zhu, FITC doped rattle-type silica colloidal particle-based ratiometric fluorescent sensor for biosensing and imaging of superoxide anion, ACS Appl. Mater. Interfaces 8 (2016) 6423–6430.
[11] Y. Liu, M. Ye, Q. Ge, X. Qu, Q. Guo, X. Hu, Q. Sun, Ratiometric quantum dot–ligand system made by phase transfer for visual detection of double-stranded DNA and single-nucleotide polymorphism, Anal. Chem. 88 (2016) 1768–1774.
[12] Y. Chen, L. Chen, Y. Ou, L. Guo, F. Fu, Enzyme-free detection of DNA based on hybridization chain reaction amplification and fluorescence resonance energy transfer, Sens. Actuators B Chem. 233 (2016) 691–696.
[13] N. Xu, J. Lei, Q. Wang, Q. Yang, H. Ju, Dendritic DNA–porphyrin as mimetic enzyme for amplified fluorescent detection of DNA, Talanta 150 (2016) 661–665.
[14] T.K. Ryan, W.Y. Jacky, B. ZhongáTang, An AIE-active fluorescence turn-on bioprobe mediated by hydrogen-bonding interaction for highly sensitive detection of hydrogen peroxide and glucose, Chem. Commun. 52 (2016) 10076–10079.
[15] Y. Cen, Y. Yang, R.Q. Yu, T.T. Chen, X. Chu, A cobalt oxyhydroxide nanoflake-based nanoprobe for the sensitive fluorescence detection of T4 polynucleotide kinase activity and inhibition, Nanoscale 8 (2016) 8202–8209.
[16] L. Liu, Q. Yang, J. Lei, N. Xu, H. Ju, DNA-regulated silver nanoclusters for label-free ratiometric fluorescence detection of DNA, Chem. Commun. 50 (2014) 13698–13701.
[17] O. Zagorodko, J. Spadavecchia, A.Y. Serrano, I. Larroulet, A. Pesquera, A. Zurutuza, R. Boukherroub, S. Szunerits, Highly sensitive detection of DNA hybridization on commercialized graphene-coated surface plasmon resonance interfaces, Anal. Chem. 86 (2014) 11211–11216.
[18] B.Y. Liu, F. Zeng, S.Z. Wu, J.S. Wang, F.C. Tang, Ratiometric sensing of mercury (II) based on a FRET process on silica core-shell nanoparticles acting as vehicles, Microchim. Acta 180 (2013) 845–853.
[19] Y. Cheng, Y. Huang, J. Lei, L. Zhang, H. Ju, Design and biosensing of Mg^{2+}-dependent DNAzyme-triggered ratiometric electrochemiluminescence, Anal. Chem. 86 (2014) 5158–5163.
[20] Q. Wang, W. Wang, J. Lei, N. Xu, F. Gao, H. Ju, Fluorescence quenching of carbon nitride nanosheet through its interaction with DNA for versatile fluorescence sensing, Anal. Chem. 85 (2013) 12182–12188.
[21] L.E. Page, X. Zhang, C.M. Tyrakowski, C.T. Ho, P.T. Snee, Synthesis and characterization of DNA–quantum dot conjugates for the fluorescence ratiometric detection of unlabelled DNA, Analyst 141 (2016) 6251–6258.
[22] J.Z. Ge, Z. Liu, Q.Y. Cao, Y. Chen, J.H. Zhu, A pyrene-functionalized polynorbornene for ratiometric fluorescence sensing of pyrophosphate, Chem. Asian J. 11 (2016) 687–690.
[23] S. Liu, J. Zhao, K. Zhang, L. Yang, M. Sun, H. Yu, Y. Yan, Y. Zhang, L. Wu, S. Wang, Dual-emissive fluorescence measurements of hydroxyl radicals using a coumarin-activated silica nanohybrid probe, Analyst 141 (2016) 2296–2302.
[24] X.F. Yan, Z.P. Chen, Y.Y. Cui, Y.L. Hu, R.Q. Yu, Quantitative generalized ratiometric fluorescence spectroscopy for turbid media based on probe encapsulated by biologically localized embedding, Anal. Chim. Acta 921 (2016) 38–45.
[25] X.T. Zheng, A. Ananthanarayanan, K.Q. Luo, P. Chen, Glowing graphene quantum dots and carbon dots: properties, syntheses, and biological applications, Small 11 (2015) 1620–1636.
[26] M. Kumar, S. Vezzoli, Z. Wang, V. Chaudhary, R.V. Ramanujan, G.G. Gurzadyan, A. Bruno, C. Soci, Hot exciton cooling and multiple exciton generation in PbSe quantum dots, Phys. Chem. Chem. Phys. 18 (2016) 31107–31114.
[27] X. Zhao, R.P. Bagwe, W. Tan, Development of organic-dye-doped silica nanoparticles in a reverse microemulsion, Adv. Mater. 16 (2004) 173–176.
[28] B.Z. Ristic, M.M. Milenkovic, I.R. Dakic, B.M. Todorovic-Markovic, M.S. Milosavljevic, M.D. Budimir, V.G. Paunovic, M.D. Dramicanin, Z.M. Markovic, V.S. Trajkovic, Photodynamic antibacterial effect of graphene quantum dots, Biomaterials 35 (2014) 4428–4435.
[29] J. Yao, K. Zhang, H. Zhu, F. Ma, M. Sun, H. Yu, J. Sun, S. Wang, Efficient ratiometric fluorescence probe based on dual-emission quantum dots hybrid for on-site determination of copper ions, Anal. Chem. 85 (2013) 6461–6468.
[30] D.R. Larson, W.R. Zipfel, R.M. Williams, S.W. Clark, M.P. Bruchez, F.W. Wise, W.W. Webb, Water-soluble quantum dots for multiphoton fluorescence imaging in vivo, Science 300 (2003) 1434–1436.
[31] H. Li, X. He, Z. Kang, H. Huang, Y. Liu, J. Liu, S. Lian, C.H.A. Tsang, X. Yang, S.T. Lee, Water-soluble fluorescent carbon quantum dots and photocatalyst design, Angew. Chem. Int. Ed. 122 (2010) 4532–4536.
[32] H. Duan, S. Nie, Etching colloidal gold nanocrystals with hyperbranched and multivalent polymers: a new route to fluorescent and water-soluble atomic clusters, J. Am. Chem. Soc. 129 (2007) 2412–2413.

[33] L. Shang, S. Dong, Sensitive detection of cysteine based on fluorescent silver clusters, Biosens. Bioelectron. 24 (2009) 1569–1573.
[34] J. Gao, K. Chen, R. Xie, J. Xie, S. Lee, Z. Cheng, X. Peng, X. Chen, Ultrasmall near-infrared non-cadmium quantum dots for in vivo tumor imaging, Small 6 (2010) 256–261.
[35] X. Gao, Y. Cui, R.M. Levenson, L.W. Chung, S. Nie, In vivo cancer targeting and imaging with semiconductor quantum dots, Nat. Biotechnol. 22 (2004) 969–976.
[36] K.D. Wegner, N. Hildebrandt, Quantum dots: bright and versatile in vitro and in vivo fluorescence imaging biosensors, Chem. Soc. Rev. 44 (2015) 4792–4834.
[37] L. Wu, X. Li, K. Shao, S. Ye, C. Liu, C. Zhang, H. Han, Enhanced immunoassay for porcine circovirus type 2 antibody using enzyme-loaded and quantum dots-embedded shell-core silica nanospheres based on enzyme-linked immunosorbent assay, Anal. Chim. Acta 887 (2015) 192–200.
[38] G. Zorn, S.R. Dave, T. Weidner, X. Gao, D.G. Castner, Direct characterization of polymer encapsulated CdSe/CdS/ZnS quantum dots, Surf. Sci. 648 (2016) 339–344.
[39] D. Gerion, F. Pinaud, S.C. Williams, W.J. Parak, D. Zanchet, S. Weiss, A.P. Alivisatos, Synthesis and properties of biocompatible water-soluble silica-coated CdSe/ZnS semiconductor quantum dots, J. Phys. Chem. B 105 (2001) 8861–8871.
[40] V.V. Goftman, T. Aubert, D.V. Ginste, R. Van Deun, N.V. Beloglazova, Z. Hens, S.D. Saeger, I.Y. Goryacheva, Synthesis, modification, bioconjugation of silica coated fluorescent quantum dots and their application for mycotoxin detection, Biosens. Bioelectron. 79 (2016) 476–481.
[41] B.H. Jun, D.W. Hwang, H.S. Jung, J. Jang, H. Kim, H. Kang, T. Kang, S. Kyeong, H. Lee, D.H. Jeong, K.W. Kang, H. Youn, D.S. Lee, Y.S. Lee, Ultrasensitive, biocompatible, quantum-dot-embedded silica nanoparticles for bioimaging, Adv. Funct. Mater. 22 (2012) 1843–1849.
[42] L. Wu, W. Yin, K. Tang, K. Shao, Q. Li, P. Wang, Y. Zuo, X. Lei, Z. Lu, H. Han, Highly sensitive enzyme-free immunosorbent assay for porcine circovirus type 2 antibody using Au-Pt/SiO_2 nanocomposites as labels, Biosens. Bioelectron. 82 (2016) 177–184.
[43] Y. Cao, L. Wen, F. Svec, T. Tan, Y. Lv, Magnetic Au NP@ Fe_3O_4 nanoparticles as reusable carriers for reversible enzyme immobilization, Chem. Eng. J. 286 (2016) 272–281.
[44] P.P. Waifalkar, S.B. Parit, A.D. Chougale, S.C. Sahoo, P.S. Patil, P.B. Patil, Immobilization of invertase on chitosan coated γ-Fe_2O_3 magnetic nanoparticles to facilitate magnetic separation, J. Colloid Interfce Sci. 482 (2016) 159–164.
[45] L. Wu, X. Xiao, K. Chen, W. Yin, Q. Li, P. Wang, Z. Lu, J. Ma, H. Han, Ultrasensitive SERS detection of Bacillus thuringiensis special gene based on Au@ Ag NRs and magnetic beads, Biosens. Bioelectron. 92 (2017) 321–327.
[46] J. Ge, Y. Hu, M. Biasini, W. Beyermann, Y. Yin, Superparamagnetic magnetite colloidal nanocrystal clusters, Angew. Chem. Int. Ed. 46 (2007) 4342–4345.
[47] L. Huang, Q. Wu, J. Wang, M. Foda, J. Liu, K. Cai, H. Han, A brilliant sandwich type fluorescent nanostructure incorporating a compact quantum dot layer and versatile silica substrates, Chem. Commun. 50 (2014) 2896–2899.
[48] M.F. Foda, L. Huang, F. Shao, H.Y. Han, Biocompatible and highly luminescent near-infrared $CuInS_2$/ZnS quantum dots embedded silica beads for cancer cell imaging, ACS Appl. Mater. Interfaces 6 (2014) 2011–2017.
[49] L. Wu, K. Chen, Z. Lu, T. Li, K. Shao, F. Shao, H. Han, Hydrogen-bonding recognition-induced aggregation of gold nanoparticles for the determination of the migration of melamine monomers using dynamic light scattering, Anal. Chim. Acta 845 (2014) 92–97.
[50] M. Martín, P. Salazar, R. Villalonga, S. Campuzano, J.M. Pingarrón, J.L. González-Mora, Preparation of core–shell Fe_3O_4@ poly (dopamine) magnetic nanoparticles for biosensor construction, J. Mater. Chem. B 2 (2014) 739–746.
[51] H.F. Cui, L. Cheng, J. Zhang, R.H. Liu, C. Zhang, H. Fan, An electrochemical DNA sensor for sequence-specific DNA recognization in a homogeneous solution, Biosens. Bioelectron. 56 (2014) 124–128.
[52] K. Chen, L. Wu, X. Jiang, Z. Lu, H. Han, Target triggered self-assembly of Au nanoparticles for amplified detection of Bacillus thuringiensis transgenic sequence using SERS, Biosens. Bioelectron. 62 (2014) 196–200.

Biographies

Long Wu was born in Hubei Province, China, in 1988. He is now a PhD in the School of Food Science and Technology at the Huazhong Agricultural University under the direction of Professor Heyou Han. His research interests focus on biosensing and bioanalysis.

Jiamin Deng was born in Inner Mongolia, China, in 1994. She is receiving his BS degree in Huazhong Agricultural University in 2017. Her research interests focus on biosensing and bioimaging.

Xuecai Tan is a Professor of Chemistry, School of Chemistry and Chemical Engineering, Guangxi University for Nationalities, China. He received his PhD degree in 2005 from Sun Yat-Sen University. His research work has been mainly focused on electroanalytical chemistry and biosensors.

Wenmin Yin was born in Jiangxi Province, China, in 1993. She received his BS degree Huazhong Agricultural University in 2015. Her research interests focus on biosensing and bioanalysis.

Fan Ding was born in Hubei Province, China, in 1994. He received his BS degree Huazhong Agricultural University in 2016. His research interests focus on biosensing and bioanalysis.

Heyou Han was born in Anhui Province, China, in 1962. He received his Ph.D. degree in Wuhan University in 2000 and he was a postdoctor in Jeckson State University (America) from 2000 to 2004. He has been a Professor of Huazhong Agricultural University since 2004. He has published over 100 papers in international journals. His research interests focus on functionalized nanomaterials for bioanalysis, food safety and energy applications.